DOI: 10.1002/chem.200601844

VIP

Iron-Catalyzed C2–C3 Bond Cleavage of Phenylpyruvate with O_2: Insight into Aliphatic C–C Bond-Cleaving Dioxygenases

Tapan Kanti Paine, Jason England, and Lawrence Que, Jr.*[a]

Abstract: Iron(II)-phenylpyruvate complexes of tetradentate tris(6-methyl-2-pyridylmethyl)amine (6-Me_3-TPA) and tridentate benzyl bis(2-quinolinylmethyl)amine (Bn-BQA) were prepared to gain insight into C–C bond cleavage catalyzed by dioxygenase enzymes. The complexes we have prepared and characterized are [Fe(6-Me_3-tpa)(prv)][BPh_4] (**1**), [Fe_2(6-Me_3-tpa)$_2$(pp)][(BPh_4)$_2$] (**2**), and [Fe_2(6-Me_3-tpa)$_2$(2′-NO_2-pp)][(BPh_4)$_2$] (**3**), [Fe(6-Me_3-tpa)(pp-Me)][BPh_4] (**4**), [Fe(6-Me_3-tpa)(CN-pp-Et)][BPh_4] (**5**), and [Fe(Bn-bqa)(pp)] (**8**), in which PRV is pyruvate, PP is the enolate form of phenylpyruvate, 2′-NO_2-PP is the enolate form of 2′-nitrophenylpyruvate, PP-Me is the enolate form of methyl phenylpyruvate, and CN-PP-Et is the enolate form of ethyl-3-cyanophenylpyruvate. The structures of mononuclear complexes **1** and **5** were determined by single-crystal X-ray diffraction. Both the PRV ligand in **1** and the CN-PP-Et ligand in **5** bind to the iron(II) center in a bidentate manner and form 5-membered chelate rings, but the α-keto moiety is in the enolate form in **5** with concomitant loss of a C–H_β proton. The PP ligands of **2**, **3**, **4**, and **8** react with dioxygen to form benzaldehyde and oxalate products, which indicates that the C2–C3 PP bond is cleaved, in contrast to cleavage of the C1–C2 bond previously observed for complexes that do not contain α-ketocarboxylate ligands in the enolate form. These reactions serve as models for metal-containing dioxygenase enzymes that catalyze the cleavage of aliphatic C–C bonds.

Keywords: bioinorganic chemistry · C–C bond cleavage · enzymes · iron · O–O activation

Introduction

Many dioxygenase enzymes catalyze the cleavage of C–C bonds, which results in the incorporation of both atoms of molecular oxygen into the oxidized substrate. Prominent among these enzymes are the catechol dioxygenases, which are mononuclear non-heme iron enzymes that catalyze oxidative ring-opening reactions of dihydroxybenzene substrates and α-keto acid dependent enzymes that couple the oxidative decarboxylation of α-keto acids with the oxidation of substrate.[1] Dioxygenase enzymes that cleave aliphatic C–C bonds of substrates that contain enolate functionalities have also been identified, such as β-diketone dioxygenase,[2,3] quercetin 2,3-dioxygenase,[4] and acireductone dioxygenase[5,6] These enzymes contain Fe, Cu, and Ni, respectively, in their active sites.

Our interest in *p*-hydroxyphenylpyruvate dioxygenase,[7] which participates in tyrosine catabolism and catalyzes the conversion of *p*-hydroxyphenylpyruvate to 2,5-dihydroxyphenylacetate, led us to investigate the iron coordination chemistry of phenylpyruvate (PPH). In the course of this investigation, we found that iron coordination of phenylpyruvate can lead to the labilization of the C3 proton to form an enolate complex. Exposure of this complex to O_2 resulted in unexpected C2–C3 bond cleavage[8] and further studies reported herein give evidence for a cleavage mechanism that can be applied to enolate-cleaving dioxygenase enzymes.

Results and Discussion

Syntheses of the complexes and their structures: Treatment of the tetradentate tris(6-methyl-2-pyridylmethyl)amine (6-Me_3-TPA) ligand and $Fe(ClO_4)_2$ with sodium pyruvate (Na(PRV)), sodium phenylpyruvate (Na(PPH)), 2′-nitrophenyl-

[a] T. K. Paine, J. England, L. Que, Jr.
Department of Chemistry and Center for Metals in Biocatalysis
207 Pleasant Street S.E., University of Minnesota
Minneapolis, MN 55455 (USA)
Fax: (+1) 612-624-7029
E-mail: que@chem.umn.edu

Supporting information for this article is available on the WWW under http://www.chemeurj.org/ or from the author. It contains the IR spectra of complexes **1**, **2**, **4**, and **8;** the variable temperature ^{1}H NMR spectra of complexes **6** and **7**; and the ^{1}H NMR spectrum of the oxidation product of complex **6**.

pyruate (Na(2′-NO_2-PPH)), methyl phenylpyruvate (H(PP-Me)), and ethyl 3-cyano-phenylpyruvate (H(CN-PP-Et)) afforded high yields of complexes **1**–**5**, respectively (Scheme 1). These pyruvate ligands bind in a κ^2 (*O,O*) manner to the mononuclear iron(II) centers of **1**, **4**, and **5**, and in a κ^3 (*O,O,O*) fashion to the diiron centers of **2** and **3**, in which a dianionic phenylpyruvate ligand bridges the two {Fe(6-Me_3-tpa)} centers. Mononuclear complex **8**, which contains dianionic phenylpyruvate, was synthesized by treating the tridentate benzyl bis(2-quinolinylmethyl)amine (Bn-BQA) ligand and $Fe(ClO_4)_2$ with sodium phenylpyruvate (Scheme 1). Oxalate-bridged diiron(II) complexes **6** and **9** were synthesized by treating sodium oxalate and $Fe(ClO_4)_2$ in methanol with 6-Me_3-TPA and Bn-BQA, respectively, to confirm the nature of the metal-containing oxidation products derived from the reactions of O_2 with **2**, **3**, and **8**. Similarly, the identity of the oxidation product of complex **4** was confirmed by comparison with complex **7**, which was prepared by treating [Fe(6-Me_3-tpa)$(OTf)_2$] with tetrabutylammonium monomethyloxalate in THF, from which it precipitates. Attempts to prepare this complex in other solvents were hampered by the observation that complex **7** was slowly converted to oxalate-bridged complex **6** upon standing in solution.

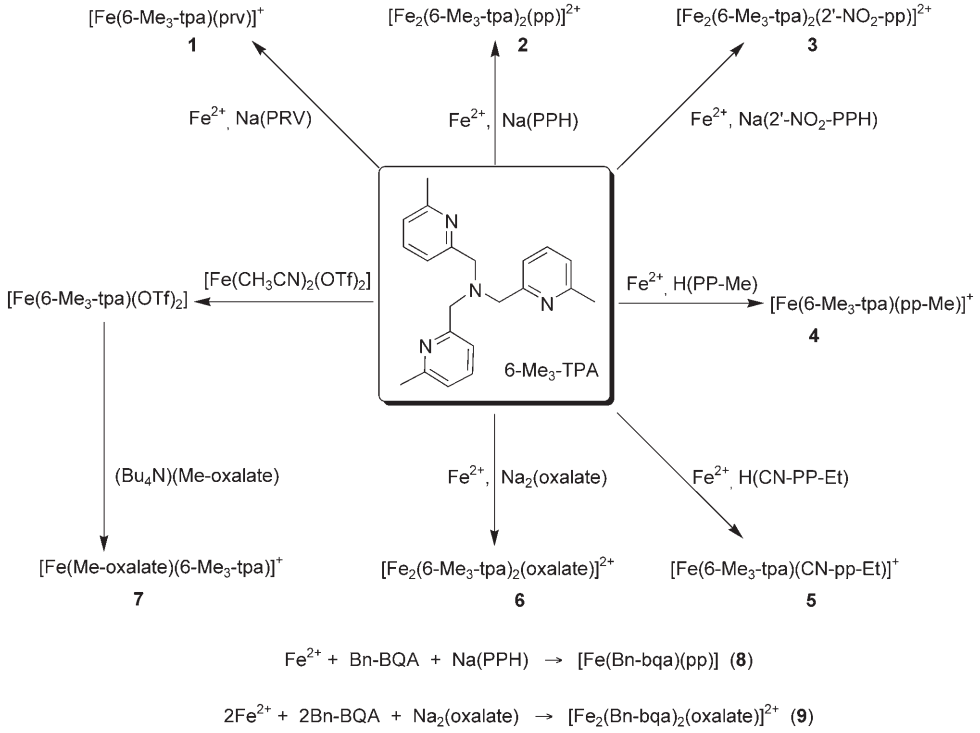

Fe^{2+} + Bn-BQA + Na(PPH) → [Fe(Bn-bqa)(pp)] (**8**)

$2Fe^{2+}$ + 2Bn-BQA + Na_2(oxalate) → $[Fe_2$(Bn-bqa)$_2$(oxalate)$]^{2+}$ (**9**)

Scheme 1. Synthesis of 6-Me_3-TPA complexes **1**–**7** and Bn-BQA complexes **8** and **9**.

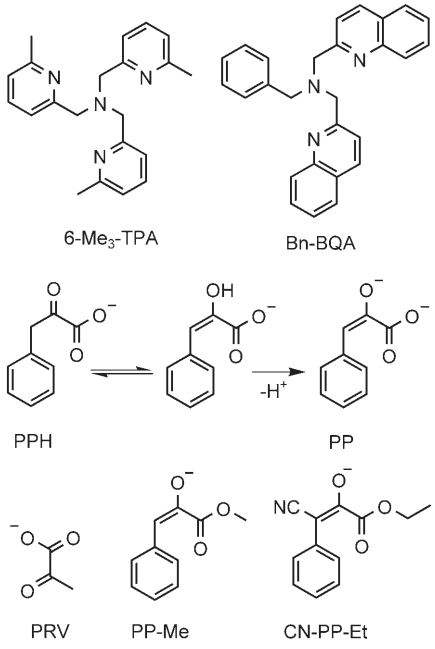

*Molecular structure of **1***: The crystal structure of **1** shows that the iron atom is in a distorted octahedron with a tetradentate tripodal ligand and a bidentate pyruvate (PRV) ligand, which is the α-keto acid functionality (Figure 1). Selected bond lengths of **1** are provided in Table 1. Pyruvate is coordinated to the iron center through a carboxylate oxygen (O1) at 1.997(4) Å and the carbonyl oxygen (O3) at 2.274(5) Å. The difference in bond length of 0.277 Å occurs as a result of the greater basicity of the carboxylate. The shorter Fe–O1 bond is *trans* to the Fe–N(amine) bond, and the longer Fe–O3 bond is *trans* to the stronger Fe–N(pyridine) bond. The C22–C23 bond length of 1.544(9) Å in the α-keto acid moiety clearly indicates the presence of a C–C single bond between the carboxylate and the α-carbonyl group. Steric interactions between the C14 α-methyl group and the C7 and C21 α-methyl groups of the 6-Me_3-TPA ligand prevent the axial pyridine nitrogen atoms from coordinating to the iron(II) center at the optimum bond length, which means that the axial Fe–N2 and Fe–N4 distances are longer than the equatorial Fe–N1 and Fe–N3 distances. The O1-Fe1-N3 angle (115.92(7)°) is significantly larger than the ideal octahedral angle (90°). Such distortions from octahedral geometry are typical for the 6-Me_3-TPA ligand and have also been observed in the $[Fe^{II}$(6-Me_3-tpa)(OBz)]-$[BPh_4]$ and $[Fe^{II}$(bf)(6-Me_3-tpa)$][ClO_4]$ complexes, in which OBz is benzoate and BF is benzoylformate.[9,10]

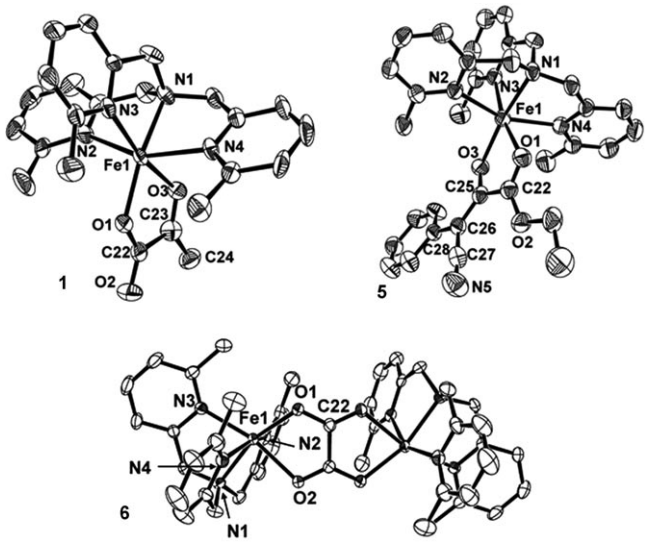

Figure 1. ORTEP representations of $[Fe(6\text{-}Me_3\text{-}tpa)(prv)]^+$ (**1**), $[Fe(6\text{-}Me_3\text{-}tpa)(CN\text{-}pp\text{-}Et)]^+$ (**5**), and $[Fe_2(6\text{-}Me_3\text{-}tpa)_2(oxalate)]^{2+}$ (**6**), which show 50% probability thermal ellipsoids. Hydrogen atoms are omitted for clarity.

Table 1. Selected bond lengths (Å) for **1**, **2**, **5**, and **6**.[a]

	1	**2** (6-coordinate Fe)	**2** (5-coordinate Fe)	**5**	**6**
Fe–O(terminal)	1.997(4) (O1)	2.219(3) (O1)		2.285(3) (O1)	2.237(3) (O2)
Fe–O(α)	2.274(5) (O3)	1.970(3) (O3)	1.988(3) (O2)	1.982(3) (O3)	2.046(3) (O1)
Fe–N(amine)	2.158(5) (N1)	2.201(4) (N1)	2.192(4) (N5)	2.169(3) (N1)	2.183(3) (N1)
Fe–N(pyridine)	2.268(5) (N2)	2.332(4) (N2)	2.229(4) (N6)	2.252(3) (N2)	2.235(4) (N2)
	2.163(5) (N3)	2.203(4) (N3)	2.101(4) (N7)	2.182(3) (N3)	2.210(4) (N3)
	2.220(5) (N4)	2.253(4) (N4)	2.187(4) (N8)	2.232(3) (N4)	2.236(4) (N4)
C(α)–O	1.231(8)	1.322(6)		1.282(5)	1.268(5)
C(terminal)–O	1.284(7)	1.259(5)	1.282(6)	1.216(5)	
C(terminal)–C(α)	1.544(9)	1.509(6)		1.515(6)	
C(α)–C(β)	1.487(10)	1.343(6)		1.371(6)	1.550(8)

[a] Terminal, α, and β labels used as shown here: 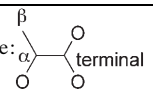

*Molecular structure of **5***: The crystal structure of monocationic **5** shows a mononuclear iron(II) complex that contains a monoanionic enolate of ethyl-3-cyanophenylpyruvate (CN-PP-Et) coordinated in a bidentate fashion (Figure 1). Selected bond lengths of **5** are provided in Table 1. The iron center is in a distorted octahedral environment with four nitrogen atoms from the tripodal ligand and a bidentate CN-PP-Et monoanion coordinated through O1 and O3. The average Fe–N bond distance of 2.21 Å is typical for high-spin $\{Fe(6\text{-}Me_3\text{-}tpa)\}$ complexes.[9,10] The Fe1–O1 distance of 2.285(3) Å is typical for an Fe^{II}–O(carbonyl) interaction, whereas the shorter Fe1–O3 distance of 1.982(3) Å is typical for a negatively charged enolate oxygen.[8] The C25–O3 bond (1.282 Å) is a C–O bond derived from CN-PP-Et. The C25–C26 distance of 1.371 (6) Å is clearly indicative of a double bond.[11] The phenyl group is almost coplanar with the α-enol carboxylate moiety, and has an O3-C25-C26-C28 torsion angle of 3.9(6)°. The short Fe1–O3 bond is *trans* to the Fe1–N(amine) bond and the longer Fe1–O1 bond is *trans* to the Fe–N(pyridine) bond. This structure resembles that previously reported for the six-coordinate iron center of **2** with a bidentate enolate form of phenylpyruvate (PP) dianion ligand (Table 1).[8]

*Molecular structure of **6***: Single-crystal X-ray structural analysis of **6** substantiates a dinuclear structure in which two distorted octahedral iron(II) ions are symmetrically bridged by an oxalate ligand (Figure 1, Table 1). The asymmetric unit contains one half of the dication. The six coordination sites of the iron(II) ions are occupied by four nitrogen atoms of the tripodal ligand and two oxygen atoms from the oxalate anion. The average Fe–N bond distance of 2.22 Å is typical for high-spin $\{Fe^{II}(6\text{-}Me_3\text{-}tpa)\}$ complexes.[9,10] The short Fe1–O1(carboxylate) bond (2.046(3) Å) is *trans* to the Fe–N1(amine) bond and the longer Fe–O2(carbonyl) bond (2.237(3) Å) is *trans* to the Fe–N3(pyridine) bond.

Spectroscopic properties of complexes: Several spectroscopic methods were useful analytical tools for further characterization of the complexes. ESI-MS analysis of **1–9** shows dominant positive ions that correspond to the cations of each complex (Table 2) and show the expected isotope distribution patterns. IR data show an intense $\tilde{\nu}$(CO) vibration at around 1690 cm^{-1} for **1**, which supports the idea that the α-keto acid moiety is maintained, whereas the absence of this characteristic vibration in **2**, **4**, and **8** is consistent with the tautomerization of the keto groups of the phenylpyruvate moieties to their enolate forms (see Figure S1 in the Supporting Information).

Complexes **1–9** exhibit distinct electronic spectra (Table 2). Light orange mononuclear complex **1** exhibits a visible transition at 485 nm ($\varepsilon = 200\ M^{-1}\ cm^{-1}$) that can be assigned as an iron(II)–α-keto carboxylate charge-transfer transition, as previously observed for other α-keto acid complexes.[12,13] This feature is blue-shifted relative to that of $[Fe^{II}(bf)(6\text{-}Me_3\text{-}tpa)]^+$, which is consistent with replacing the phenyl group with the more electron-donating methyl group. The absorption intensity is almost half that of those reported for benzoylformate compounds owing to the loss of conjugation of the α-keto acid chromophore with the aromatic ring, which is almost coplanar with the chelated α-keto carboxylate in benzoylformate complexes. Complex **1** also exhibits a near-UV transition at 368 nm ($\varepsilon = 1700\ M^{-1}\ cm^{-1}$) that can be assigned to an iron(II)–pyridine charge-transfer transition, as found for related Fe^{II}–tpa complexes in which TPA is tris(2-pyridylmethyl)amine.[9,14] The

Table 2. ESI-MS and optical spectral data for complexes **1**–**9** in CH_3CN.[a]

Complex	Formula	m/z[b]	λ_{max} [nm] (ε [$M^{-1}cm^{-1}$])	Reaction time with O_2
1	$[C_{24}H_{27}FeN_4O_3]^+$	475.2	368(1700), 485(200)	–[c]
2	$[C_{51}H_{54}Fe_2N_8O_3]^{2+}$	469.2 (dication)	332(22000), 440(1800)	15 min
3	$[C_{51}H_{53}Fe_2N_9O_5]^{2+}$	491.6 (dication)	327(16600), 395(6600)	45 min
4	$[C_{31}H_{33}FeN_4O_3]^+$	565.2	336(20600), 420(1700)	3 h
5	$[C_{33}H_{34}FeN_5O_3]^+$	604.2	338(13000), 420(1200)	–[c]
6	$[C_{44}H_{48}Fe_2N_8O_4]^{2+}$	432.2 (dication)	370(3000)	–[c]
7	$[C_{24}H_{27}FeN_4O_4]^+$	491.2		–[c]
8	$[C_{36}H_{29}FeN_3O_3]+H^+$	608.2	338(8000), 440(1000)	1 h
9	$[C_{56}H_{46}Fe_2N_6O_4]^{2+}$	489.2 (dication)	398(1800), 450(1300)	–[c]
2+OBz	$[C_{28}H_{29}FeN_4O_2]^+$	509.2	323(25000)	2.5 h
	$[C_{30}H_{30}FeN_4O_3]+H^+$	551.2		

[a] See Scheme 1 for the compositions of these complexes. [b] Recorded in positive mode. [c] No reaction was observed.

same assignment can be made for the band at 370 nm (ε = 3000 $M^{-1}cm^{-1}$) observed for the oxalate-bridged diiron(II) complex **6**.

Complexes **2**–**5** and **8** exhibit spectra that are quite different from that of **1**. They have UV transitions at around 330 nm that are much more intense ($\varepsilon \approx 8000$–20000 $M^{-1}cm^{-1}$) and an additional band at around 400 nm. On the other hand, unlike other models for α-keto acid-dependent enzymes, complexes **2**–**5** do not have features between 540 and 610 nm, which have been assigned to iron(II)–α-keto carboxylate charge-transfer bands,[9,15,16] because the α-keto group has tautomerized to its more conjugated enolate form upon complex formation. Thus, the features at around 330 and 400 nm are likely to arise from enolate–iron(II) interactions. In support of this hypothesis, we noted that the visible transition of **2** at 440 nm (shoulder; ε = 1800 $M^{-1}cm^{-1}$) blueshifted to 395 nm in **3** and more than tripled in intensity ($\varepsilon \approx 6600\ M^{-1}cm^{-1}$) when a nitro substituent on the phenyl ring of the conjugated enolate was introduced.

Complexes **1**–**6** all have high-spin Fe^{II} centers that give rise to paramagnetically shifted ^{1}H NMR signals in the range of $\delta = -60$ to 150 ppm. The spectrum of **1** resembles that of $[Fe^{II}(bf)(6\text{-}Me_3\text{-}tpa)]^+$ and peak assignments for the ligand protons were made by comparisons with that complex. Figures 2 and 3 show the ^{1}H NMR spectra of **2**, **4**, **6**, and **7** and the chemical shifts and assignments for **1**–**4** are listed in Table 3 for comparison with those of the other complexes. Owing to its simplicity, the spectrum of **4** (Figure 2, bottom) will be discussed first. Complex **4** contains pyridine α-CH_3 protons that are shifted upfield to δ = −28 and −48 ppm and have a 2:1 intensity ratio. Four well-resolved peaks with appropriate intensity ratios are observed in the region of δ = 33–55 ppm and are assigned as the β and β′ protons of the pyridines, whereas the pyridine γ protons are found at δ = 9.0 ppm. The C3–H enolate proton from the enolate form of methylphenylpyruvate (PP-Me) experiences an upshift to $\delta = -48$ ppm to coincide with one set of α-CH_3 protons, and the carbomethoxy protons are found at 12.4 ppm.

In the ^{1}H NMR spectrum of **2** (Figure 2, top), there are three sets of pyridine peaks observed in a 1:2:3 ratio. The two sets of peaks with a 1:2 ratio are assigned as the octahedral Fe1, which has an approximate plane of symmetry defined by N1, N3, and the enolate ligand. The remaining peaks are then assigned as the five-coordinate Fe2 site, which is, unsurprisingly, fluxional on the NMR timescale. The *ortho*, *meta*, and *para* protons of the phenylpyruvate moiety in **2** are found at δ = −3.6, 16.0, and −6.3 ppm, respectively. The shifts observed are larger than those associated with the phenyl protons in BF complexes. This alternating upfield–downfield–upfield shift pattern is typical of a dominant π-delocalization mechanism,[17] which is consistent with the extended π-conjugation associated with the enolate form. Consistent with sign alternation pattern, the C3–H

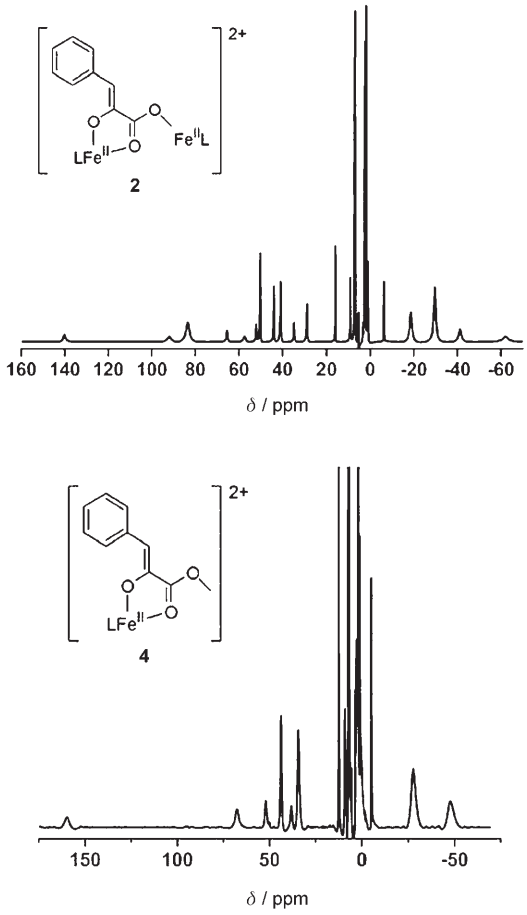

Figure 2. ^{1}H NMR spectra of $[Fe_2(6\text{-}Me_3\text{-}tpa)_2(pp)][(BPh_4)_2]$ (**2**) and $[Fe(6\text{-}Me_3\text{-}tpa)(pp\text{-}Me)][BPh_4]$ (**4**) in CD_3CN at room temperature.

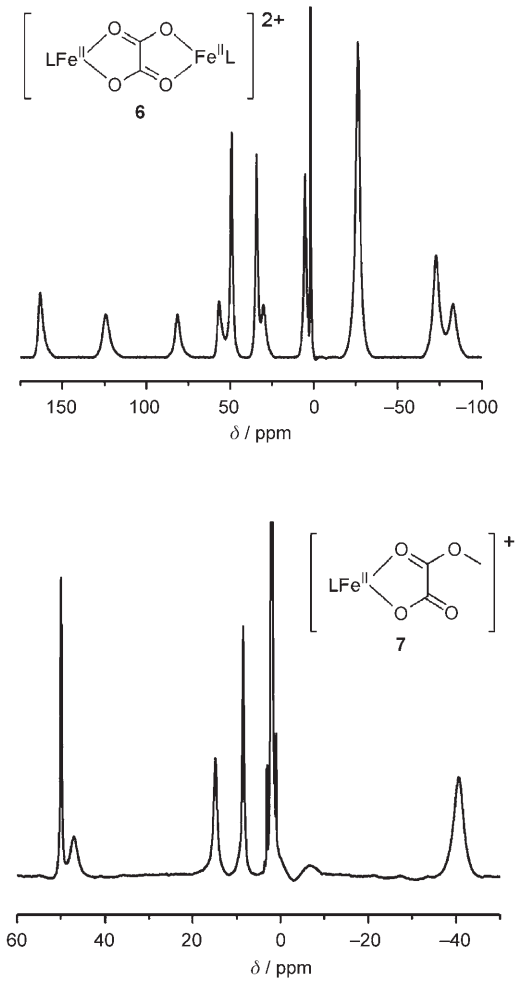

Figure 3. ^{1}H NMR spectra of $[Fe_2(6\text{-}Me_3\text{-}tpa)_2(oxalate)](ClO_4)_2$ (**6**) and [Fe(Me-oxalate)(6-Me_3-tpa)][OTf] (**7**) in CD_3CN at room temperature.

proton experiences an even larger upshift of $\delta = -62$ ppm. Similar features are observed for **3** (Table 3).

On the other hand, the ^{1}H NMR spectra of complexes **6** and **7** (Figure 3) are more difficult to assign. Despite the use of analytically pure material, complex **6** exhibits more resonances than expected based upon the symmetry found in its crystal structure, which implies that the solid state structure is not maintained in solution. Additionally, attempts to assign the spectrum based upon the assumption that it represented the presence of a single species were unsuccessful. Variable temperature (VT) ^{1}H NMR experiments (see Figure S2 in the Supporting Information) demonstrate that the room temperature spectrum reflects a partly coalesced fluxional mixture of at least three distinct species, based upon the number of pyridyl α-Me resonances. This fluxional behavior presumably derives from the potential coordinative flexibility of the oxalate ligand (i.e. monodentate vs. bidentate and bridging vs. nonbridging) in combination with the inherent high lability of the high-spin iron(II) centers.

In contrast to that of complex **6**, the ^{1}H NMR spectrum of complex **7** (Figure 3, bottom) has an insufficient number of

Table 3. ^{1}H NMR parameters of **1**–**4**.

Assignments	**1**[a]	**2**[a]	**3**[a]	**4**[a]
CH_2		140.2 (2H)	147.9 (2H)	159.6 (3H)
		92.0 (2H)	98.0 (2H)	67.6 (3H)
		83.5 (6H)	76.2 (6H)	
		65.5 (2H)	68.2 (2H)	
αCH_3	−36.4 (9H)	−18.6 (6H)	−22.9 (6H)	−47.7 (3H)
		−29.6 (9H)	−25.0 (9H)	−27.6 (6H)
		−41.2 (3H)	−48.6 (3H)	
py β, β′	49.4 (6H)	52.0 (1H)	52.7 (1H)	52.0 (1H)
		50.3 (3H)	50.4 (3H)	43.7 (2H)
		44.0 (2H)	45.1 (2H)	38.1 (1H)
		40.9 (3H)	40.4 (3H)	34.4 (2H)
		34.7 (1H)	34.2 (1H)	
		28.8 (2H)	28.3 (2H)	
py γ	17.2 (3H)	9.1 (2H)	9.0 (2H)	9.0 (3H)
		7.2 (4H)	7.2 (4H)	
2-NO_2-PP[b] (or PP *o*-H)		−3.6 (2H)	−4.7 (1H)	−4.9 (2H)
2-NO_2-PP[b] (or PP *m*-H)		16.0 (2H)	15.6 (1H)	
			12.6 (1H)	
2-NO_2-PP[b] (or PP *p*-H)		−6.3 (1H)	−6.5 (1H)	
2-NO_2-PP[b] (or PP CH)		−62.1 (1H)	−65.4 (1H)	−47.7(1H)
OCH_3 of PP-Me				12.4 (3H)
CH_3 of PRV	14.6 (3H)			

[a] Chemical shift data given in ppm. [b] Enolate form of 2′-nitrophenylpyruvate.

resonances to account for all the chemically distinct proton environments in the molecule. The presence of only a single pyridine α-CH_3 peak at $\delta = -41$ ppm (cf. the two peaks seen for mononuclear complex **4**) suggests that the apparent simplicity of the spectrum is the consequence of a highly fluxional structure. This proposition was confirmed by conducting VT NMR experiments on **7**, which yielded spectra at low temperatures with strong superficial similarities to that seen for complex **6** at ambient temperatures (see Figure S3 in the Supporting Information). This apparent spectral similarity indicates that, regardless of the differing nuclearity of the two complexes in the solid state, the fluxional processes exhibited by them in the solution are likely to be of a similar nature. Although we were unable to make full and accurate signal assignments for the ^{1}H NMR spectra of complexes **6** and **7**, they are distinct, and hence, diagnostic of their formation as products in the oxygenation reactions discussed below.

Reactivity with dioxygen: It has been previously reported that the (benzoylformato)iron(II) complex of the 6-Me_3-TPA ligand reacts with dioxygen over a period of one week to give the decarboxylated product.[9] This slow reaction of the species with dioxygen is ascribed to its coordinatively saturated iron(II) center. On the other hand, complex **1** does not react with dioxygen under the same reaction conditions.

In contrast, **2** and **3** do react with dioxygen in MeCN at 25 °C and the reaction goes to completion in less than an hour, as monitored by the loss of their characteristic UV bands at around 330 nm (Figure 4). ESI-MS analysis of the

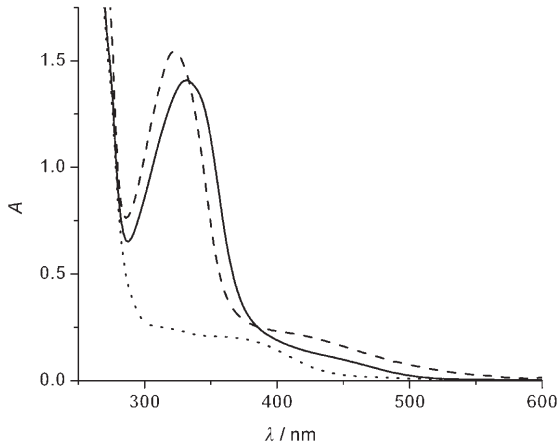

Figure 4. UV/Vis spectra of **2** (0.3 mM, 0.2 cm) in CH_3CN (——), after treatment with $(Et_4N)OBz$ (1 equiv; – – –), and after exposure to O_2 at room temperature to form **6** (·····).

product solutions showed a signal at *m*/*z* 432.2 and NMR spectra that correspond to those of **6** (Tables 2 and 3). The yield of **6** was estimated to be 80–85% by ^1H NMR spectroscopy. The only difference between the two complexes is that **2** reacts with O_2 over a period of 15 min and **3** reacts three times more slowly, owing to the presence of the NO_2 substituent on the aromatic ring of the PP moiety in **3**. GC and GC-MS analyses carried out to identify the organic products showed the formation of benzaldehyde and 2-nitrobenzaldehyde from **2** and **3**, respectively, in about 85% yield. These results indicated that the activation of dioxygen by complexes **2** and **3** resulted in C2–C3 bond cleavage of the phenylpyruvate ligand to afford oxalate and benzaldehyde or 2-nitrobenzaldehyde (Scheme 2).

The fate of dioxygen was established by $^{18}O_2$-labeling experiments. The ESI-MS spectra of the product solutions from the oxidation of **2** and **3** in the presence of $^{18}O_2$ show a major ion signal at *m*/*z* 433.2, which is one mass unit higher than that found for unlabeled **6**. This result clearly demonstrated that the oxalate bridged diron(II) product contained

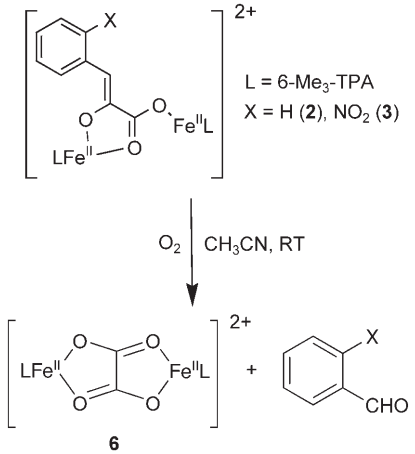

Scheme 2. Reactions of **2** and **3** with dioxygen in acetonitrile.

one atom of oxygen from dioxygen. The other ^{18}O atom was incorporated into benzaldehyde. GC-MS analysis showed 82% incorporation of ^{18}O; some loss of label from $PhCH^{18}O$ may have resulted from exchange with trace amounts of $H_2{}^{16}O$ present in the MeCN solvent.

To simplify the system and determine if the dimeric form of the complex was important for oxidative C–C bond cleavage, **2** was treated with tetraethylammonium benzoate (1 equiv) in acetonitrile at ambient temperature under an inert atmosphere to detach the five-coordinate Fe(L) unit. A slight blue shift of the UV band was observed (Figure 4, dashed line). ESI-MS analysis of the solution showed two major signals at *m*/*z* 551.2 and 509.2, which had the expected isotope distribution patterns that corresponded to $[Fe^{II}(6\text{-}Me_3\text{-tpa})(pp)+H]^+$ and $[Fe^{II}(6\text{-}Me_3\text{-tpa})(OBz)]^+$, respectively (Scheme 3). This solution reacts with dioxygen over a period of 2.5 h to give complex **6** and benzaldehyde. The yield of benzaldehyde was 76% based on diiron(II) complex **2**. The monoiron(II)-benzoate complex does not react with oxygen and remains unchanged after the oxidation process.

It is important to note that complex **2** was the only product isolated from the reaction of $\{Fe^{II}(6\text{-}Me_3\text{-tpa})\}$ with phenylpyruvate and no mononuclear Fe^{II}–pp complex of the tetradentate 6-Me_3-TPA ligand could be synthesized or isolated. One strategy to avoid the formation of the dimeric phenylpyruvate complex is to use the phenylpyruvate ester as a ligand in which a carboxylate oxygen is protected by an alkyl group and thus, is prevented from coordinating to another $\{Fe(6\text{-}Me_3\text{-tpa})\}$ unit. Indeed only mononuclear Fe^{II} complexes are formed with methyl or ethyl phenylpyruvate substrates. One such mononuclear iron(II) complex, **4**, reacted with dioxygen in MeCN over a period of 3 h to produce a yellow solution that had an ESI-mass spectrum with a signal at *m*/*z* 491.2, which corresponded to the molecular

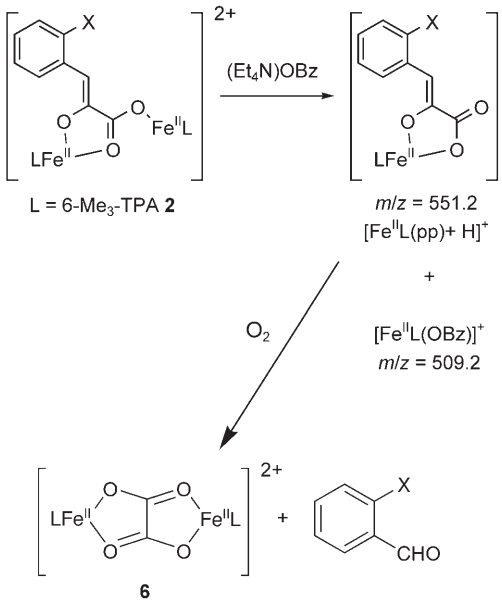

Scheme 3. Reactivity of **2** with dioxygen in the presence of $(Et_4N)OBz$ in acetonitrile.

ion of **7** (Scheme 4). The ^{1}H NMR spectrum of the final reaction solution (see Figure S4 in the Supporting Information) matched that of complex **7** prepared independently,

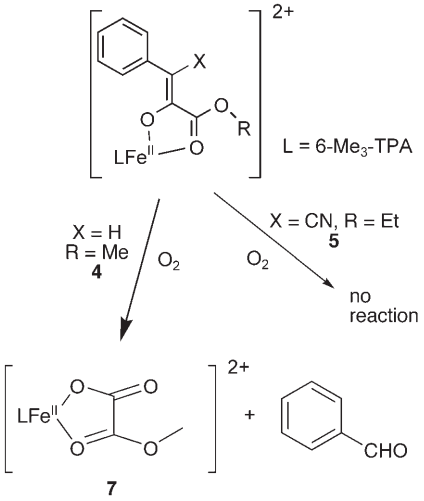

Scheme 4. Reactivity of methyl or ethyl phenylpyruvate complexes with dioxygen.

which confirmed the formation of the proposed product from the oxygenation of **4**. The organic product was benzaldehyde, as expected, and was obtained in 71% yield. On the other hand, complex **5** does not react with dioxygen under the same conditions (Scheme 4). We attribute this lack of reactivity to the presence of the electronegative cyano group, which reduces the electron density at the C=C bond and prevents dioxygen activation.

Complex **8** also reacts with dioxygen in MeCN over a period of 1 h (Figure 5) to afford a yellow solution that had an ESI-MS signal at *m*/*z* 489.2 and an NMR spectrum that matched that obtained for **9**. The NMR spectrum suggested that **9** was formed in about 80% yield, whereas benzaldehyde, identified by GC analysis, was obtained in 70% yield.

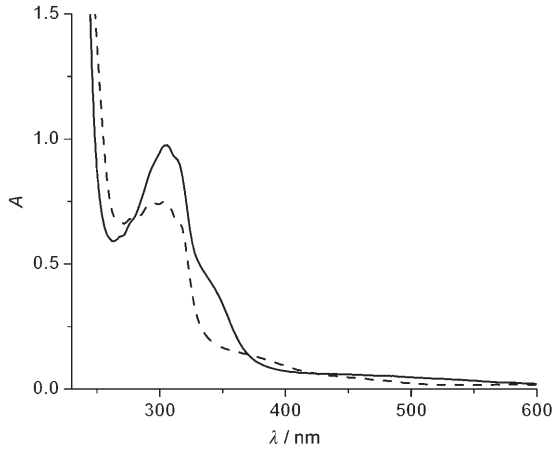

Figure 5. UV/Vis spectra of **8** (0.3 mM, 0.2 cm) in CH_3CN (——) and after exposure to O_2 at room temperature to form **9** (– – –).

The ESI-MS spectrum recorded for the solution of **8** after oxidation with $^{18}O_2$ had a major ion signal at *m*/*z* 490.2, which had an isotope distribution pattern that indicated 80% incorporation of ^{18}O. This result clearly demonstrated that the oxalate bridged diron(II) product contained one atom of oxygen from dioxygen (Scheme 5). The other ^{18}O

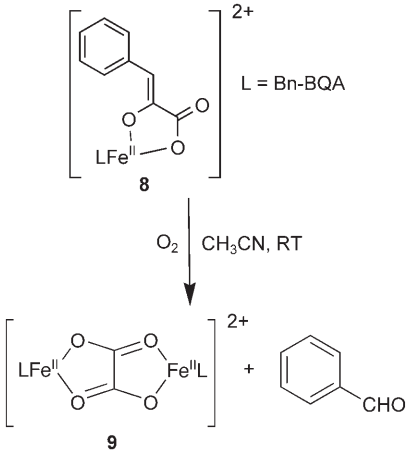

Scheme 5. Reaction of **8** with dioxygen in acetonitrile.

atom was incorporated into the benzaldehyde byproduct to a similar extent (80%), as established by GC-MS analysis.

All the PP enolate complexes, except for the cyano derivative, react with dioxygen to undergo C2–C3 bond cleavage within 3 h (Table 2). Surprisingly, complex **2** has the shortest reaction time of 15 min, which is tenfold shorter than its mononuclear counterparts, **2**+OBz and **4**. Even **8**, which has a coordinatively unsaturated iron(II) center, reacts fourfold more slowly. Based on these observations, we postulate that the initial attack of O_2 takes place not at the metal center, but at the C3 carbon of the coordinated enolate to form an oxygenated PP intermediate, which leads to cleavage of the C2–C3 and O–O bonds in subsequent steps, to afford the final products (Scheme 6). Kinetic analysis of these reactions may provide more insight.

The C2–C3 cleavage reactivity we have observed for the enolate forms of the phenylpyruvate complexes is reminiscent of biodegradative non-heme enzymes that catalyze aliphatic C–C bond cleavage, such as iron-requiring β-diketone dioxygenase,[2,3] copper-requiring quercetin 2,3-dioxygenase,[4] and nickel-requiring acireductone dioxygenase.[5,6] All these transformations involve substrates that contain enolate functionalities. From these observations, we postulate that an important role of the metal center in these non-heme enzymes is to promote formation of the enolate form of the substrate, which increases electron density at the enolate β-carbon and renders it susceptible to attack by O_2. The paramagnetic nature of the metal center may also promote reaction with O_2 because no Zn-dependent enzymes with a similar function have been identified to date. The results reported in this paper support this mechanistic postulate and

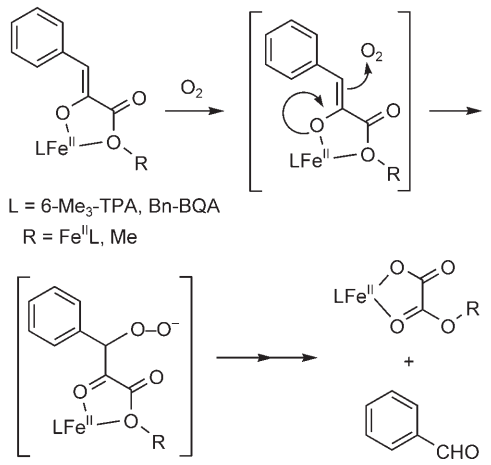

Scheme 6. Proposed mechanism for oxidative C=C bond cleavage.

demonstrate the key role that coordination chemistry can play in directing the course of an oxidative transformation.

Experimental Section

General: All reagents and solvents were purchased from commercial sources and were used without further purification, unless otherwise noted. Thiophene-free benzene, diethyl ether, and tetrahydrofuran were distilled from sodium/benzophenone ketyl under an argon atmosphere prior to use. Dichloromethane and acetonitrile were carefully purified by distillation under an argon atmosphere from CaH_2.[18] Methanol was distilled from $Mg(OMe)_2$ before use. Preparation and handling of air-sensitive materials were carried out under an inert atmosphere by using standard Schlenk techniques or a glove box. *Although no problems were encountered during the synthesis of these complexes from $Fe(ClO_4)_2$, perchlorate salts are potentially explosive and should be handled with care.*[19] Ligands 6-Me_3-TPA[20] and Bn-BQA[14] were prepared as previously reported. Methyl phenylpyruvate[21] and potassium monomethyloxalate[22] were synthesized according to literature procedures.

General procedure for the synthesis of complexes 1–5: Equimolar amounts (0.25 mmol) of 6-Me_3-TPA, phenylpyruvate, and $Fe(ClO_4)_2{\cdot}6H_2O$ in MeOH (5 mL) were stirred under argon for 2 h. The resulting solution was then treated with a solution of $NaBPh_4$ (0.25 mmol) in methanol to precipitate the microcrystalline solid, which was isolated by filtration, washed with methanol, and dried.

*[Fe(6-Me_3-tpa)(prv)][BPh_4] (**1**)*: Yield: 0.12 g (60%). X-ray quality crystals were grown by vapor diffusion of diethyl ether into a solution of **1** in dichloromethane. Elemental analysis calcd (%) for $C_{48}H_{47}BFeN_4O_3$: C 72.56, H 5.96, N 7.05; found: C 72.42, H 5.87, N 7.11.

*[Fe_2(6-Me_3-tpa)$_2$(pp)][(BPh_4)$_2$] (**2**)*: Yield: 0.15 g (76%); elemental analysis calcd (%) for $C_{99.5}H_{95}B_2ClFe_2N_8O_3$: C 73.79, H 5.91, N 6.92; found: C 74.19, H 5.95, N 6.96.

*[Fe_2(6-Me_3-tpa)$_2$(2′-NO_2-pp)][(BPh_4)$_2$] (**3**)*: Yield: 0.18 g (91%); elemental analysis calcd (%) for $C_{99.5}H_{94}B_2ClFe_2N_9O_5$: C 71.79, H 5.69, N 7.57; found: C 71.80, H 5.66, N 7.61.

*[Fe(6-Me_3-tpa)(pp-Me)][BPh_4] (**4**)*: Yield: 0.16 g (73%); elemental analysis calcd (%) for $C_{55}H_{53}BFeN_4O_3$: C 74.67, H 6.04, N 6.33; found: C 75.00, H 6.09, N 6.37.

*[Fe(6-Me_3-tpa)(CN-pp-Et)][BPh_4] (**5**)*: Yield: 0.15 g (65%). X-ray quality crystals were grown by vapor diffusion of diethyl ether into a solution of **5** in dichloromethane. Elemental analysis calcd (%) for $C_{57.75}H_{55.5}BCl_{1.5}FeN_5O_3$: C 70.25, H 5.67, N 7.09; found: C 70.47, H 5.62, N 7.01.

*[Fe_2(6-Me_3-tpa)$_2$(oxalate)][(ClO_4)$_2$] (**6**)*: Equimolar amounts (0.25 mmol) of 6-Me_3-TPA, sodium oxalate, and $Fe(ClO_4)_2{\cdot}6H_2O$ in MeOH (5 mL) were stirred under argon. The solution turned yellow immediately and a yellow microcrystalline solid precipitated, which was isolated by filtration, washed with methanol, and dried (0.11 g, 85%). Elemental analysis calcd (%) for $C_{44}H_{48}Cl_2Fe_2N_8O_{12}$: C 49.69, H 4.55, N 10.54; found: C 49.39, H 4.75, N 10.16.

($NnBu_4$)(Me-oxalate): A mixture of tetrabutylammonium chloride (0.50 g, 1.80 mmol) and potassium monomethyloxalate (0.26 g, 1.80 mmol) in methanol (15 mL) was stirred for 30 minutes before the solvent was removed in vacuo. Addition of CH_2Cl_2 (50 mL) to the resulting residue, filtration, and concentration of the filtrate yielded an oil that solidified upon drying under vacuum (0.46 g, 74%). The highly hygroscopic nature of the off-white solid obtained prevented accurate measurement by elemental analysis. ^{1}H NMR ($CDCl_3$): $\delta = 3.68$ (s, 3H; *Me*O), 3.33 (t, 2H; NC*H*$_2$), 1.64 (pent, 2H; NCH$_2$C*H*$_2$), 1.41 (m, 2H; NCH$_2$CH$_2$C*H*$_2$), 0.97 ppm (t, 3H; NCH$_2$CH$_2$CH$_2$C*H*$_3$); ^{13}C NMR ($CDCl_3$): $\delta = 166.7$, 162.7, 58.6, 53.3, 23.8, 19.5, 13.5 ppm; elemental anal-

Table 4. Summary of Crystallographic Data for [Fe(6-Me_3-tpa)(prv)][BPh_4] (**1**), [Fe(6-Me_3-tpa)(CN-pp-Et)](BPh_4) (**5**)·CH_2Cl_2, and [Fe_2(6-Me_3-tpa)$_2$(oxalate)][(ClO_4)$_2$] (**6**)·CH_2Cl_2.

	1	**5**·CH_2Cl_2	**6**·CH_2Cl_2
formula	$C_{48}H_{47}BFeN_4O_3$	$C_{58}H_{56}BCl_2FeN_5O_3$	$C_{45}H_{49}Cl_4Fe_2N_8O_{12}$
M_r [g mol^{-1}]	794.56	1008.64	1147.42
crystal color	red	yellow	yellow
crystal system	orthorhombic	triclinic	orthorhombic
space group	$P2_12_12_1$	$P\bar{1}$	*P*nna
a [Å]	9.540(2)	12.7625(18)	16.3730(14)
b [Å]	13.510(3)	13.9179(19)	24.283(2)
c [Å]	31.320(7)	16.773(2)	12.6777(11)
α [°]	90	79.068(2)	90
β [°]	90	75.022(2)	90
γ [°]	90)	64.242(2)	90)
V [Å^3]	4036.5(16)	2581.9(6)	5040.6(8)
Z	4	2	4
ρ_{calcd} [g cm^{-3}]	1.307	1.297	1.512
T [K]	173(2)	173(2)	173(2)
absorption coefficient [mm^{-1}]	0.422	0.445	0.856
θ [°]	1.30 to 25.05	1.26 to 25.09	1.68 to 25.04
limiting indices	$-10<h<11$	$-15<h<15$	$0<h<19$
	$-16<k<16$	$-16<k<16$	$0<k<28$
	$-37<l<37$	$-19<l<19$	$0<l<15$
reflns collected	28471	23790	39094
unique reflns	7127 ($R_{int}=0.0740$)	9119 ($R_{int}=0.0449$)	4459 ($R_{int}=0.1152$)
observed reflns ($I>2\sigma(I)$)[a]	5720	5703	3021
parameters/restraints	519/12	635/0	346/62
R_1/wR_2 ($I>2\sigma(I)$)[a]	0.0749, 0.1854	0.0593, 0.1541	0.0654, 0.1074
R_1/wR_2 (all data)	0.0958, 0.1971	0.1102, 0.1855	0.1089, 0.1206
goodness-of-fit on F^2	1.043	1.049	1.074
max/min peak [e Å^3]	1.029/−0.745	0.504/−0.811	0.613/−0.570

[a] $R_1=\Sigma\,||F_o|-|F_c||/\Sigma|F_o|$. $wR_2=\{\Sigma[w(F_o^2-F_c^2)^2]/\Sigma[w(F_o^2)^2]\}^{1/2}$ in which $w=q/\sigma^2(F_o^2)+(a*P)^2+b*P$. GOF = $\{\Sigma[w(F_o^2-F_c^2)^2]/(n-p)\}^{1/2}$.

ysis calcd (%) for $C_{19}H_{39}NO_4$: C 66.05, H 11.38, N 4.05; found: C 65.50, H 11.89, N 4.22.

[Fe(6-Me$_3$-tpa)(OTf)$_2$]: An equimolar quantity (3.00 mmol) of [Fe(CH$_3$CN)$_2$(OTf)$_2$] and 6-Me$_3$-TPA were dissolved in THF (35 mL) and allowed to stir overnight. Reduction of the volume of solution to around 10 mL and addition of diethyl ether (40 mL) gave the product as a white precipitate, which was isolated by filtration and dried in vacuo (1.90 g, 92%). The ^{1}H NMR spectrum recorded in CD$_3$CN solution was identical to that previously reported for [Fe(CH$_3$CN)$_2$(6-Me$_3$-tpa)][(ClO$_4$)$_2$].[9,10,20] Elemental analysis calcd (%) for $C_{23}H_{26}F_6FeN_4O_7S_2$: C 39.22, H 3.72, N 7.95; found: C 39.31, H 3.60, N 7.93.

*[Fe(Me-oxalate)(6-Me$_3$-tpa)][OTf] (**7**)*: Equimolar amounts (0.29 mmol) of [Fe(6-Me$_3$-tpa)(OTf)$_2$] and tetrabutylammonium monomethyloxalate were dissolved in THF (10 mL) and stirred under argon for 1 h, during which time an egg-yolk yellow precipitate formed. The solid was subsequently isolated by filtration, washed with THF, and dried under vacuum (0.12 g, 63%). Elemental analysis calcd (%) for $C_{25}H_{27}F_3FeN_4O_7S$: C 46.89, H 4.25, N 8.75; found: C 47.31, H 4.53, N 8.50.

*[Fe(Bn-bqa)(pp)] (**8**)*: A solution of Fe(ClO$_4$)$_2$·6H$_2$O (0.10 g, 0.25 mmol) in methanol (2 mL) was added dropwise to a mixture of Bn-BQA (0.0897 g, 0.25 mmol) and Na(PPH) (0.05 g, 0.25 mmol) in methanol (3 mL). The red solution was stirred at room temperature for 1 h and a red microcrystalline solid separated from the solution that was isolated by filtration, washed with methanol, and dried (0.10 g, 67%). Elemental analysis calcd (%) for $C_{36}H_{29}FeN_3O_3$: C 71.18, H 4.81, N 6.92; found: C 71.42, H 4.87, N 7.03.

*[Fe$_2$(Bn-bqa)$_2$(oxalate)](ClO$_4$)$_2$ (**9**)*: Compound **9** was obtained in a similar manner to **6**, except that Bn-BQA was used as the ligand instead of 6-Me$_3$-TPA. The solid was recrystallized from a 1:1 mixture of CH$_2$Cl$_2$/diethyl ether (0.14 g, 95%). Elemental analysis calcd (%) for $C_{56}H_{46}Cl_2Fe_2N_6O_{12}\cdot{}^3/_2CH_2Cl_2$: C 52.92, H 3.87, N 6.44; found: C 52.99, H 4.09, N 6.49.

Physical studies: Elemental analyses were determined by Atlantic Microlab. The IR spectra were measured as KBr pellets by using a Perkin–Elmer 1600 Series FTIR instrument in the range of $\tilde{\nu}$ = 4000 to 400 cm^{-1}. Electrospray ionization mass spectral data were collected by using a Bruker BioTOF MS instrument equipped with ESI, and samples were introduced by direct infusion by using a syringe pump. Room temperature UV/Vis spectra were recorded by using an HP 8452 A diode array spectrometer that contained a temperature-controlled bath set at 25 °C. All room temperature ^{1}H NMR spectra were collected by using a Varian VI-500 spectrometer. VT ^{1}H NMR measurements were made by using a Varian VI-300 spectrometer. Chemical shifts (ppm) for complexes were referenced to the residual solvent. Special care was taken to ensure that the delay between pulses was greater than five times the longest proton longitudinal relaxation time (T_1) for proper integration of the peaks. GC mass spectral analyses were performed by using an HP 5898 GC (DB-5 column, 60 m) instrument with a Finnigan MAT 95 mass detector or an HP 6890 GC (HP-5 column, 30 m) instrument with an Agilent 5973 mass detector. A 4% NH_3/CH_4 mixture was used as the ionization gas for chemical ionization analyses.

Identification of organic products: In a typical reaction, 2 mL of a 5 mM solution of the appropriate phenylpyruvate complex (**2**, **4**, or **8**) in MeCN, maintained at 25 °C, was bubbled with O_2 and then stirred under O_2 for 3 h. Naphthalene (13.7 mM, 0.5 mL) was added as an internal standard to this reaction solution. The reaction solution was then passed through a short silica column, washed thoroughly with MeCN, and analyzed by GC. The product was identified by comparing its GC retention time with that of authentic compound and quantified relative to the internal standard.

X-ray crystallographic data collection and refinement of the structures of 1, 5, and 6: Each crystal was attached to the tip of a glass capillary by using heavy-weight oil and mounted on a Siemens SMART Platform CCD diffractometer for data collection at 173(2) K by using graphite-monochromated $Mo_{K\alpha}$ radiation (λ = 0.71073 Å). An initial set of cell constants was calculated from reflections harvested from three sets of 20 frames. These initial sets of frames were oriented such that orthogonal wedges of reciprocal space were surveyed; this produced initial orientation matrices determined from 64 reflections for **1**, 12 reflections for **5**, and 330 reflections for **6**. Crystallographic data and experimental conditions are summarized in Table 4. All non-hydrogen atoms were refined anisotropically and hydrogen atoms were placed in ideal positions and refined as riding atoms with relative isotropic displacement parameters. The final full-matrix least-squares refinement converged to R_1 = 0.0749 and wR_2 = 0.1971 for **1**, R_1 = 0.0593 and wR_2 = 0.1855 for **5**, and R_1 = 0.0654 and wR_2 = 0.1206 for **6**. CCDC-290342, -290343, and -290341 contain the supplementary crystallographic data for **1**, **5**, and **6**, respectively. These data can be obtained free of charge from the Cambridge Crystallographic Data Centre via www.ccdc.cam.ac.uk/data_request/cif.

Acknowledgements

This work was supported by the National Institutes of Health (GM-33162). We thank Dr. Victor G. Young, Jr., Benjamin Kucera, and William W. Brennessel of the University of Minnesota X-ray Crystallographic Laboratory for determining the crystal structures of **1**, **5**, and **6**.

[1] M. Costas, M. P. Mehn, M. P. Jensen, L. Que, Jr., *Chem. Rev.* **2004**, *104*, 939.
[2] G. D. Straganz, H. Hofer, W. Steiner, W. B. Nidetzky, *J. Am. Chem. Soc.* **2004**, *126*, 12202.
[3] G. D. Straganz, B. Nidetzky, *J. Am. Chem. Soc.* **2005**, *127*, 12306.
[4] R. A. Steiner, K. H. Kalk, B. W. Dijkstra, *Proc. Natl. Acad. Sci. USA* **2002**, *99*, 16625.
[5] T. C. Pochapsky, S. S. Pochapsky, T. Ju, H. Mo, F. Al-Mjeni, M. J. Maroney, *Nat. Struct. Biol.* **2002**, *9*, 966.
[6] F. J. Al-Mjeni, T. Ju, T. C. Pochapsky, M. J. Maroney, *Biochemistry* **2002**, *41*, 6761.
[7] K. Johnson-Winters, V. M. Purpero, M. Kavana, T. Nelson, G. R. Moran, *Biochemistry* **2003**, *42*, 2072.
[8] T. K. Paine, H. Zheng, L. Que, Jr., *Inorg. Chem.* **2005**, *44*, 474.
[9] Y.-M. Chiou, L. Que, Jr., *J. Am. Chem. Soc.* **1995**, *117*, 3999.
[10] J. Kim, Y. Zang, M. Costas, R. G. Harrison, E. C. Wilkinson, L. Que Jr, J. Biol. Inorg. Chem. **2001**, *6*, 276.
[11] B. M. Gatehouse, M. J. O'Connor, *Acta Crystallogr., Sect. B: Struct. Crystallogr. Cryst. Chem.* **1976**, *B32*, 3145.
[12] E. L. Hegg, R. Y. N. Ho, L. Que, Jr., *J. Am. Chem. Soc.* **1999**, *121*, 1972.
[13] M. P. Mehn, K. Fujisawa, E. L. Hegg, L. Que, Jr., *J. Am. Chem. Soc.* **2003**, *125*, 7828.
[14] S. V. Kryatov, S. Taktak, I. V. Korendovych, E. V. Rybak-Akimova, J. Kaizer, S. Torelli, X. Shan, S. Mandal, V. L. MacMurdo, A. Mairata i Payeras, L. Que, Jr., *Inorg. Chem.* **2005**, *44*, 85.
[15] E. G. Pavel, N. Kitajima, E. I. Solomon, *J. Am. Chem. Soc.* **1998**, *120*, 3949.
[16] R. Y. N. Ho, M. P. Mehn, E. L. Hegg, A. Liu, M. J. Ryle, R. P. Hausinger, L. Que, Jr., *J. Am. Chem. Soc.* **2001**, *123*, 5022.
[17] L.-J. Ming in *Physical Methods in Bioinorganic Chemistry. Spectroscopy and Magnetism* (Ed.: L. Que, Jr.), University Science Books, Sausalito, CA, **2000**, p. 375.
[18] W. L. F. Armarego, D. D. Perrin, *Purification of Laboratory Chemicals*, Butterworth-Heinemann, Oxford, **1997**.
[19] W. C. Wolsey, *J. Chem. Educ.* **1973**, *50*, A335.
[20] Y. Zang, J. Kim, Y. Dong, E. C. Wilkinson, E. H. Appelman, L. Que, Jr., *J. Am. Chem. Soc.* **1997**, *119*, 4197.
[21] M. F. Brana, M. L. Garcia, B. Lopez, B. de Pascual-Teresa, A. Ramos, J. M. Pozuelo, M. T. Dominguez, *Org. Biomol. Chem.* **2004**, *2*, 1864.
[22] K. Nagao, N. Saraumi, (Daiso), JP 03223231, **1991** [*Chem. Abstr.* **1992**, *117*, 47934].

Received: December 21, 2006
Published online: April 27, 2007

